DEU FMD 27(80) (2025) 257-266

Dokuz Eylül Üniversitesi Mühendislik Fakültesi Fen ve Mühendislik Dergisi
Dokuz Eylul University Faculty of Engineering Journal of Science and Engineering
Elektronik/Online ISSN: 2547-958X

RESEARCH ARTICLE / ARAŞTIRMA MAKALESI

Internal Damping Instability of Rotors with Isotropic and Anisotropic Supports based on Complex Coordinates Formulation

Kompleks Koordinat Formülasyonuna Dayalı İzotropik ve Anizotropik Mesnetli Rotorların İç Sönümleme Kararsızlığı

Furkan Çopur, Saeed Lotfan *

Department of Mechanical Engineering, Gebze Technical University, Kocaeli, Turkey
Corresponding Author / Sorumlu Yazar *: slotfan@gtu.edu.tr

Abstract

This study investigates the advantages and disadvantages of complex coordinates formulation for internal damping stability of rotordynamic systems. Damping mechanisms inherent to the rotor structure have different effects on vibrations when compared to stationary damping sources. The internal and external damping sources experience different vibration frequencies with respect to the stationary reference frame. Thus, in contrast to external damping, internal damping does not always stabilize vibrations. Therefore, the correct incorporation of damping forces into the model is investigated to predict vibration characteristics accurately. A unified finite element model is developed to study rotordynamic stability due to internal damping caused by frictional joints between rotor parts and structural damping. Rotating bearing elements are used to model internal frictional joints and the governing equation with hysteresis damping is provided using complex vector notation for rotors on isotropic and anisotropic mounts. Complex coordinates formulation provides mathematical advantages in transformation of vectors between rotating and stationary reference frames. In the case of isotropic supports, the use of complex coordinates formulation yields a low-dimensional model and increases the efficiency of the model. However, in the case of anisotropic supports, reduction in the order of the model is not possible and the equation of motion is nonlinear due to kinematics of the system. This requires an iterative method to solve the eigenvalue problem. For verifications, the results of the developed models are compared to those of a commercial finite element software. Consequently, the effect of different internal damping sources on the overall rotordynamic stability is demonstrated.

Keywords: *Rotordynamics, internal damping stability, complex coordinates formulation, frictional joints, structural damping*

Öz

Bu çalışma, rotordinamik sistemlerin iç sönümleme kararlılığı için kompleks koordinat formülasyonunun avantaj ve dezavantajlarını araştırmaktadır. Rotor yapısına özgü sönümleme mekanizmaları, sabit sönümleme kaynaklarına kıyasla titreşimler üzerinde farklı etkilere sahiptir. İç ve dış sönümleme kaynakları, sabit referans çerçevesine göre farklı titreşim frekanslarına sahiptir. Bu nedenle, harici sönümlemenin aksine, dahili sönümleme titreşimleri her zaman kararlı hale getirmez. Bu nedenle, titreşim özelliklerini doğru bir şekilde tahmin etmek için sönümleme kuvvetlerinin modele doğru bir şekilde dahil edilmesi araştırılmıştır. Rotor parçaları arasındaki sürtünme bağlantılarının ve yapısal sönümlemenin neden olduğu iç sönümleme nedeniyle rotordinamik kararlılığı incelemek için birleşik bir sonlu eleman modeli geliştirilmiştir. İç sürtünme bağlantılarını modellemek için döner yatak elemanları kullanılmış ve histerezis sönümlemeli dinamik denklemi, izotropik ve anizotropik bağlantılar üzerindeki rotorlar için karmaşık vektör gösterimi kullanılarak sağlanmıştır. Kompleks koordinat formülasyonu, dönen ve sabit referans çerçeveleri arasındaki vektörlerin dönüşümünde matematiksel avantajlar sağlamaktadır. İzotropik mesnetler söz konusu olduğunda, kompleks koordinat formülasyonunun kullanılması düşük boyutlu bir model ortaya çıkarmakta ve modelin verimliliğini artırmaktadır. Ancak, anizotropik mesnetler söz konusu olduğunda, modelin mertebesinin azaltılması mümkün olmamakta ve sistemin kinematiği nedeniyle hareket denklemi doğrusal değildir. Bu durum, özdeğer problemini çözmek için iteratif bir yöntem gerektirmektedir. Doğrulama için, geliştirilen modellerin sonuçları ticari bir sonlu elemanlar yazılımının sonuçları ile karşılaştırılmıştır. Sonuç olarak, farklı iç sönümleme kaynaklarının genel rotordinamik kararlılık üzerindeki etkisi gösterilmiştir.

Anahtar Kelimeler: *Rotordinamik, iç sönüm kararlılığı, kompleks koordinat formülasyonu, sürtünmeli mafsallar, yapısal sönümleme*

1. Introduction

Rotating machines have been widely studied theoretically and experimentally in the past decades as the most common mechanical system. There are many aspects to this research content, including modal analysis [1], fault detection [2], stability [3], blade dynamics [4], and nonlinear vibrations [5] to name a few. Despite the abundant number of studies carried out in this area, developing precise models to evaluate the stability characteristics retains this research area as one of the important ongoing research topics.

Gyroscopic and circulatory effects are the two most important differences between the lateral vibrations of a rotordynamic system and a generic vibration problem [6]. Gyroscopic effects appear due to Coriolis reactions within a vibratory mode shape [7], causing a frequency separation between forward and backward modes with rotor speed. On the other hand, circulatory

DOI: https://doi.org/10.21205/deufmd.2025278012

Geliş Tarihi / Received: 04.03.2024
Kabul Tarihi / Accepted: 09.09.2024

terms arise during the transformation of the rotating damping forces to stationary reference frame. Circulatory terms are the reason for the difference between the effect of internal and external damping on the vibration behavior of the rotordynamic system. Internal damping does not always have a stabilizing effect on vibrations, unlike external damping. Vibration problems arise when circulatory terms dominate the external damping forces in super-critical operations. This phenomenon is also known as internal rotordynamic instability.

The first family of internal instability sources involves frictional joints between rotor parts [8]. Certain design characteristics of turbomachinery rotors result in a relative slip between rotor surfaces. Most notable design features that will lead to rotordynamic instability are axial splines, interference fits and curvic couplings. Built-up rotors, where different rotating parts are connected via shrink fits and pretensioned tie-shafts, are particularly susceptible to stability issues. As pioneer studies in this field, Lund [9] and Walton et.al. [10] studied the impact of these features on the internal rotordynamic stability. In their studies, these features are modelled as angular stiffness and damping coefficients. It is assumed that stiffness of joints contributes to elastic forces, while frictional forces due to relative slip act as rotating damping force. A rotordynamic model should have the capability of modelling the stiffness and damping between two mating rotor surfaces to accurately capture circulatory effects. Recently, nonlinear transient analysis is performed by Wang et.al [11] to show the effect of internal damping on the stability threshold of a built-up rotors on nonlinear journal bearings. Dai et.al. [12] experimentally studied the effect of different spline characteristics on rotor stability. Experiments are performed for different lubrication, external damping, load, teeth profile and fit type conditions. They concluded that well lubricated and properly loaded splines provide better stability performance.

The second major source of internal instability is hysteresis damping of rotor material, which is generally modelled as proportional to stiffness with a structural damping coefficient, normalized with frequency to achieve a damping force independent of frequency. This normalization is a controversial topic in rotordynamic literature. Analytical solution for the internally damped rotating Timoshenko shaft is presented by Melanson and Zu [13]. Their results showed that internal viscous damping is destabilizing at super-critical speeds while hysteretic damping is destabilizing at all speeds. Many authors employed numerical techniques with similar mathematical foundations to demonstrate the impact of internal viscous and hysteretic damping [14, 15]; several of which concluded the destabilizing effect of hysteretic damping at all speeds [16, 17]. On the other hand, Genta explained the misunderstanding on internal instability due to hysteretic damping [18]. He stated that hysteretic and viscous damping play the same role from a stability perspective. Like viscous damping, hysteretic damping does not induce instability in the sub-critical regime as well. Neglecting the difference between the frequencies of the hysteretic and vibration cycles, which are not coincident for rotating systems, was the main source of erroneous result in the previous literature. Genta later provided a more detailed explanation, accompanied by example case studies featuring advanced hysteresis damping models [19]. Then, he covered the stability of rotors on asymmetric mounts as well [20]. D'Alessandro et al. [21] utilized Genta's approach [18] later to compare the effect of viscous and hysteresis damping on rotordynamic stability. Despite the extensive literature background, even the most widely used commercial finite element software still lacks the accurate implementation of hysteretic damping in rotordynamic modelling. To achieve a unified modelling method to study internal rotordynamic study, accurate modelling of hysteretic damping plays a crucial role.

Most of the studies in the literature on the internal damping instability problem of rotordynamic systems are based on real coordinates systems [11, 22-25]. However, as an alternative approach, one can utilize complex coordinates formulation to model the problem. In this approach, real and imaginary parts of a complex degree of freedom (DoF) represent vibration in each lateral plane, which imply a rotating vector. This assumption provides a mathematical advantage in the modelling of rotating bodies while transforming vectors between stationary and rotating reference frames. When eigenvalues are calculated by employing complex coordinates, the sign of the eigenvalues show the whirl direction. This information makes the identification of forward and backward modes easier and enables the computation of relative frequency between rotating and stationary forces, which is the main source of the erroneous modeling of the structural damping in the literature. This formulation is introduced to model rotors on isotropic supports [26] and has been used in a few number of research works to study the internal and external damping in rotor systems [27, 28]. The primary motivation for this study arises from the limited number of investigations employing the complex coordinates formulation for rotors with isotropic supports. Furthermore, there is a notable scarcity of research focused on utilizing the complex coordinates formulation for rotors with anisotropic supports.

In this work, a finite element model which can accurately predict the internal stability of rotordynamic systems is developed. Timoshenko shaft elements are used to model rotor parts. Rotating bearing elements are used to model the circulatory terms due to internal damping of the frictional joints between rotor parts. The developed method is also capable of modelling hysteretic damping due to rotor and stator materials separately. The equation of motion is provided for rotors on isotropic supports by using complex coordinates showing all these various damping and circulatory terms explicitly. Mass, damping, gyroscopic, stiffness and circulatory matrices are provided for shaft elements. Equation of the motion is then extended to rotors on anisotropic supports, which requires special care when working with complex coordinates. Capabilities of the developed finite element method are demonstrated through example problems. Natural frequencies, critical speeds and decay rates are calculated based on the developed methodology. Consequently, the effect of different internal damping sources on the overall rotordynamic stability is illustrated through the comparison of decay rate plots for rotors featuring various internal damping configurations. A unified modelling method, utilizing a complex coordinates formulation, is presented to encompass various internal damping configurations.

2. Model Development of Rotors on Isotropic Supports

The developed finite element model is based on Timoshenko shaft elements with uniform cross-sections which has two translational and two rotational DoF at each station. Shaft element supports shear, rotary inertia, and gyroscopic effects. Shape functions are provided for shaft elements in the literature [29-31] and used successfully throughout the years. A shaft element has one station at each end as shown in Figure 1.

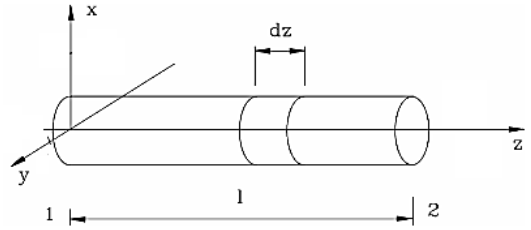

Figure 1. Timoshenko shaft element of length l [30].

The displacement vector of a shaft element in complex vector notation has the form of Equation (1). A minus sign is added to account opposite directions of the rotational DoF of right-handed coordinates system, to use same shape functions in both lateral planes.

$$\mathrm{q_{shaft}} = \{u_1 + \hat{\imath}\, v_1\,;\ \psi_1 - \hat{\imath}\, \theta_1\,;\ u_2 + \hat{\imath}\, v_2\,;\ \psi_2 - \hat{\imath}\, \theta_2\} \tag{1}$$

Here $\hat{\imath}$ represents the imaginary numbers, u is displacement in the x direction, v denotes displacement in the y direction. Moreover, ψ and θ are rotations about y and x directions, respectively. Shape functions provide the nondimensional relation between the internal deformation of a finite element and the deformations of end stations. The computation of kinetic and potential energies for an element yields stiffness and mass matrices, forming the foundation of finite element discretization. These shape functions incorporate shear deformation which prevents shear-locking problems that may otherwise lead to an overestimation of the shaft stiffness. For a more detailed understanding of these shape functions, readers are kindly referred to [31], with the details not reiterated here for the sake of brevity. Accordingly, one can express the deformations in the shaft element as:

$$\begin{Bmatrix} u \\ \psi \end{Bmatrix} = \begin{bmatrix} N_{11} & N_{12} & N_{13} & N_{14} \\ N_{21} & N_{22} & N_{23} & N_{24} \end{bmatrix} \begin{Bmatrix} u_1 \\ \psi_1 \\ u_2 \\ \psi_2 \end{Bmatrix} \tag{2a}$$

$$\begin{Bmatrix} v \\ -\theta \end{Bmatrix} = \begin{bmatrix} N_{11} & N_{12} & N_{13} & N_{14} \\ N_{21} & N_{22} & N_{23} & N_{24} \end{bmatrix} \begin{Bmatrix} v_1 \\ -\theta_1 \\ v_2 \\ -\theta_2 \end{Bmatrix} \tag{2b}$$

Here in-plane deformations, (u, ψ), are considered in Equation (2a), and out-of-plane deformations, (v, θ), are given in Equation (2b). The deformation vectors for these cases are respectively, shown by q_x and q_y in the following sections. As a result, potential energy, which eventually yields stiffness matrix can be expressed as:

$$U = \frac{1}{2}\mathrm{q_x^T K_{Shaft} q_x} + \frac{1}{2}\mathrm{q_y^T K_{Shaft} q_y} \tag{3a}$$

$$\begin{aligned} U = \frac{EI}{2L}\Bigg(& \int_0^l \mathrm{q_x^T}\frac{\mathrm{dN_2^T}}{\mathrm{d}z}\frac{\mathrm{dN_2}}{\mathrm{d}z}\mathrm{q_x}\,\mathrm{d}z \\ & + \int_0^l \mathrm{q_y^T}\frac{\mathrm{dN_2^T}}{\mathrm{d}z}\frac{\mathrm{dN_2}}{\mathrm{d}z}\mathrm{q_y}\,\mathrm{d}z\Bigg) \\ + \frac{6\mathrm{EI}}{\Phi \mathrm{L}}\Bigg(& \int_0^l \mathrm{q_x^T N_3^T N_3\, q_x}\,\mathrm{d}z + \int_0^l \mathrm{q_y^T N_3^T N_3\, q_y}\,\mathrm{d}z\Bigg) \end{aligned} \tag{3b}$$

Here, $\mathrm{N_1}$ and $\mathrm{N_2}$ denote the first and second rows of the shape function matrix in Equation (2), and $\mathrm{N_3}$ represents only the shear component of the deformation, calculated as:

$$\mathrm{N_3} = \mathrm{N_2} - \frac{\mathrm{dN_1}}{\mathrm{d}z} \tag{4}$$

Moreover, in Equation (3b), Φ is slenderness ratio defined by

$$\Phi = \frac{EI\chi}{GAl^2} \tag{5}$$

Where χ is the shear factor of a shaft with circular cross-section with inner radius r_i and outer radius r_o:

$$\begin{aligned} \frac{1}{\chi} = & \frac{7r_i^4 + 34r_i^2r_o^2 + 7r_o^4 + \nu\left(12r_i^4 + 48r_i^2r_o^2 + 12r_o^4\right)}{6\left(r_i^2 + r_o^2\right)^2(1+\nu^2)^2} \\ & + \frac{\nu^2\left(4r_i^4 + 16r_i^2r_o^2 + 4r_o^4\right)}{6\left(r_i^2 + r_o^2\right)^2(1+\nu^2)^2} \end{aligned} \tag{6}$$

With ν being the Poisson ratio of the shaft. Similarly, kinetic energy of the shaft element can be written as:

$$\begin{aligned} \mathrm{T} = & \frac{1}{2}\dot{\mathrm{q}}_\mathrm{x}^\mathrm{T}\,\mathrm{M_T}\,\dot{\mathrm{q}}_\mathrm{x} + \frac{1}{2}\dot{\mathrm{q}}_\mathrm{y}^\mathrm{T}\,\mathrm{M_T}\,\dot{\mathrm{q}}_\mathrm{y} + \frac{1}{2}\dot{\mathrm{q}}_\mathrm{x}^\mathrm{T}\,\mathrm{M_R}\,\dot{\mathrm{q}}_\mathrm{x} \\ & + \frac{1}{2}\dot{\mathrm{q}}_\mathrm{y}^\mathrm{T}\,\mathrm{M_R}\,\dot{\mathrm{q}}_\mathrm{y} + \rho J_y l\Omega^2 - 2\Omega\dot{\mathrm{q}}_\mathrm{y}^\mathrm{T}\,\mathrm{M_R}\,\dot{\mathrm{q}}_\mathrm{x} \end{aligned} \tag{7a}$$

$$\begin{aligned} \mathrm{T} = & \frac{1}{2}\rho Al\int_0^l\left(\dot{\mathrm{q}}_\mathrm{x}^\mathrm{T}\,\mathrm{N_1^T N_1}\,\dot{\mathrm{q}}_\mathrm{x} + \dot{\mathrm{q}}_\mathrm{y}^\mathrm{T}\,\mathrm{N_1^T N_1}\,\dot{\mathrm{q}}_\mathrm{y}\right)\mathrm{d}z \\ & + \frac{1}{2}\rho Il\int_0^l\left(\dot{\mathrm{q}}_\mathrm{x}^\mathrm{T}\,\mathrm{N_2^T N_2}\,\dot{\mathrm{q}}_\mathrm{x} + \dot{\mathrm{q}}_\mathrm{y}^\mathrm{T}\,\mathrm{N_2^T N_2}\,\dot{\mathrm{q}}_\mathrm{y}\right)\mathrm{d}z \\ & + \rho J_y l\Omega^2 - 2\rho J_y l\Omega\int_0^l\left(\dot{\mathrm{q}}_\mathrm{y}^\mathrm{T}\,\mathrm{N_2^T N_2}\,\dot{\mathrm{q}}_\mathrm{x}\right)\mathrm{d}z \end{aligned} \tag{7b}$$

Here, M_T and M_R are mass matrices associated with translational and rotational inertia, respectively. Kinetic energy incorporates a term related to the Coriolis effect, which is proportional to the rotor speed and eventually becomes gyroscopic matrix in the final equation of the motion. It is noteworthy that despite a shaft element having eight DoF, all element matrices are presented below as 4x4 due to the utilization of complex vector notation leading to identical matrices in in-plane and out-of-plane directions.

$$\mathrm{K}_{shaft} = \frac{EI}{(1+\Phi)l^3}\begin{bmatrix} 12 & 6l & -12 & 6l \\ 6l & (4+\chi)l^2 & -6l & (2-\chi)l^2 \\ -12 & -6l & 12 & -6l \\ 6l & (2-\chi)l^2 & -6l & (4+\chi)l^2 \end{bmatrix} \tag{8}$$

$$\mathrm{M}_T = \frac{\rho Al}{840(1+\Phi)^2}\begin{bmatrix} m_1 & m_2 & m_3 & m_4 \\ m_2 & m_5 & -m_4 & m_6 \\ m_3 & -m_4 & m_1 & -m_2 \\ m_4 & m_6 & -m_2 & m_5 \end{bmatrix} \tag{9}$$

$$\mathrm{M}_R = \frac{\rho I}{30l(1+\Phi)^2}\begin{bmatrix} m_7 & m_8 & -m_7 & m_8 \\ m_8 & m_9 & -m_8 & m_{10} \\ -m_7 & -m_8 & m_7 & -m_8 \\ m_8 & m_{10} & -m_8 & m_9 \end{bmatrix} \tag{10}$$

Mass parameters in the translational mass matrix are given by:

$$\begin{aligned} m_1 &= 312 + 588\Phi + 280\Phi^2 \\ m_2 &= (44 + 77\Phi + 35\Phi^2)l \\ m_3 &= 108 + 252\Phi + 140\Phi^2 \\ m_4 &= -(26 + 63\Phi + 35\Phi^2)l \\ m_5 &= (8 + 14\Phi + 7\Phi^2)l^2 \\ m_6 &= -(6 + 14\Phi + 7\Phi^2)l^2 \end{aligned} \tag{11}$$

Moreover, mass parameters in the rotational mass matrix are defined by:

$$\begin{aligned} m_7 &= 36 \\ m_8 &= (3 - 15\Phi)l \\ m_9 &= (4 + 5\Phi + 10\Phi^2)l^2 \\ m_{10} &= (-1 - 5\Phi + 5\Phi^2)l^2 \end{aligned} \tag{12}$$

Accordingly, mass matrix of the shaft element can be expressed as:

$$\mathrm{M}_{\mathrm{shaft}} = \mathrm{M}_T + \mathrm{M}_R \tag{13}$$

Moreover, based on the kinetic energy the gyroscopic matrix is defined by:

$$G_{shaft} = 2\mathrm{M}_R \tag{14}$$

Now, one can assemble the element matrices to form the global mass, damping and stiffness matrices to construct the mathematical model of the system. In the process of calculating the global matrices, shaft matrix is integrated with additional concentrated mass, stiffness, and dampers, which are models of disks and bearings in the rotor system. Accordingly, the general equation of motion of an isotropic system can be obtained as:

$$\begin{aligned}\mathrm{M}\ddot{\mathrm{q}} + \Big(\mathrm{C}_{bs} + \mathrm{C}_{br} + \frac{\eta_s}{|\omega|}\mathrm{K}_{bs} + \frac{\eta_r}{|\omega-\Omega|}(\mathrm{K}+\mathrm{K}_{br}) \\ - \hat{\imath}\Omega\mathrm{G}\Big)\dot{\mathrm{q}} \\ + \Big(\mathrm{K} + \mathrm{K}_{bs} + \mathrm{K}_{br} \\ - \hat{\imath}\Omega\frac{\eta_r}{|\omega-\Omega|}(\mathrm{K}+\mathrm{K}_{br}) - \hat{\imath}\Omega\mathrm{C}_{br}\Big)\mathrm{q} \\ = \left(\mathrm{f}_x + \hat{\imath}\mathrm{f}_y\right)(\Omega^2 - \hat{\imath}\,\dot{\Omega})e^{\hat{\imath}\Omega t}\end{aligned} \tag{15}$$

In which the characteristics of rotating and stationary bearings are distinguished with "*r*" and "*s*" subscripts. The subscript "*b*" is employed to differentiate bearing-related matrices from rotor-related matrices. Structural damping coefficients, η, are defined for rotor and stator parts separately. An unbalance force is also introduced to the right-hand side to account rotor speed- and acceleration-dependent excitation terms. Speed-dependent terms incorporated into the stiffness matrices represent circulatory effects induced by internal damping sources. A critical aspect of this equation lies in the definition of structural damping. The structural damping terms are normalized with frequency because structural damping remains nearly constant over a wide frequency range. However, it is essential to consider rotor speed in the transformation of rotating structural damping into the stationary reference frame. Complex coordinates become mandatory at this point since the sign of the eigenvalues represent the whirl direction in this equation. This directional information is lost when equation of motion is constructed with real coordinates. It should also be mentioned that as discussed in the introduction, neglecting the relative frequency of rotating damping has been a primary reason for erroneous results in the literature [18]. Moreover, structural damping ratios of rotor and stators are handled separately in Equation (15), which allows inclusion of corresponding circulatory terms in stiffness matrix accurately.

Furthermore, the equation of motion incorporates a rotating viscous damping matrix, denoted as C_{br}. Coefficients due to concentrated damping forces between two stations are defined between related DoF's in this matrix. This matrix also contributes to the speed-dependent circulatory terms in the stiffness matrix. It is crucial to note that both viscous and structural forms of rotating damping exert a destabilizing effect. Therefore, accurate formulation of these damping terms in the system matrices is critical for the proper detection and analysis of rotordynamic instability. Stability of the system is determined by solving for the eigenvalues of the homogeneous form of Equation (15), with the assumption of the solution in the following form:

$$\mathrm{q}(t) = \mathrm{q}_0 e^{\hat{\imath}\Omega t} \tag{16}$$

Here Ω is a complex eigenvalue, the real part of which represents the natural frequencies, and the imaginary part denotes decay rate of the free response [32-34].

3. Model Development of Rotors on Anisotropic Supports

As seen in the previous section, the use of complex coordinates systems for isotropic supports results in lower matrix dimensions, and whirl directions are obtained automatically with eigenvalue problem solution. In the case of anisotropic supports, the use of the complex coordinates formulation becomes complicated. The complex coordinates defined in Equation (1) automatically assumes that deflections in lateral planes are symmetric, in other words rotor whirls in circular orbits. This provides a computational advantage in isotropic systems since it halves the matrix sizes due to symmetry. Although the rotor is assumed to be isotropic here, anisotropy can be introduced to the system with asymmetrical rotor supports, which will result in elliptical whirl orbits. The difficulty with complex coordinates can be overcome by defining the elliptical motion as a summation of two counter-rotating circles.

$$\mathrm{q}(t) = \mathrm{q}_1(t) + \mathrm{q}_2(t) = \mathrm{q}_{1_0} e^{\hat{\imath}\Omega t} + \mathrm{q}_{2_0} e^{-\hat{\imath}\Omega t} \tag{17}$$

The introduction of anisotropic stiffness, damping, and mass characteristics of mounts in in-plane and out-of-plane directions is accomplished by defining mean and deviatoric matrices as [31]:

$$\mathrm{K}_m = \frac{1}{2}\left(\mathrm{K}_x + \mathrm{K}_y\right) + \frac{1}{2}\hat{\imath}\left(\mathrm{K}_{yx} - \mathrm{K}_{xy}\right) \tag{18a}$$

$$\mathrm{K}_d = \frac{1}{2}\left(\mathrm{K}_x - \mathrm{K}_y\right) + \frac{1}{2}\hat{\imath}\left(\mathrm{K}_{yx} + \mathrm{K}_{xy}\right) \tag{18b}$$

Although only stiffness matrices are presented here, the same definitions apply to mass and damping matrices. Despite the utilization of complex coordinates, there is no necessity to work with complex matrices for isotropic systems. However, when anisotropic supports are introduced, computations involving complex numbers become necessary due to imaginary terms in mean and deviatoric matrices. When general solution in the form of Equation (17) and new matrices of Equation (18) are introduced into the system, system size is doubled, and the equation of motion can be written as Equation (19).

$$\begin{aligned}\left(\begin{bmatrix}M & 0\\ 0 & M\end{bmatrix} + \begin{bmatrix}M_{b_m} & M_{b_d}\\ \bar{M}_{b_d} & \bar{M}_{b_m}\end{bmatrix}\right)\begin{Bmatrix}\ddot{q}_1\\ \ddot{\bar{q}}_2\end{Bmatrix} + \left(\begin{bmatrix}C_{bs_m} & C_{bs_d}\\ \bar{C}_{bs_d} & \bar{C}_{bs_m}\end{bmatrix}\right. \\ + \frac{\eta_s}{|\omega|}\begin{bmatrix}K_{bs_m} & K_{bs_d}\\ \bar{K}_{bs_d} & \bar{K}_{bs_m}\end{bmatrix} - \hat{\imath}\Omega\begin{bmatrix}G & 0\\ 0 & -G\end{bmatrix} \\ + \begin{bmatrix}C_{b_r} & 0\\ 0 & C_{b_r}\end{bmatrix} + \eta_r\left(\begin{bmatrix}\alpha K & 0\\ 0 & \beta K\end{bmatrix}\right. \\ \left.\left. + \begin{bmatrix}\alpha K_{b_r} & 0\\ 0 & \beta K_{b_r}\end{bmatrix}\right)\right)\begin{Bmatrix}\dot{q}_1\\ \dot{\bar{q}}_2\end{Bmatrix} \\ + \left(\begin{bmatrix}K & 0\\ 0 & K\end{bmatrix} + \begin{bmatrix}K_{bs_m} & K_{bs_d}\\ \bar{K}_{bs_d} & \bar{K}_{bs_m}\end{bmatrix}\right. \\ + \begin{bmatrix}K_{b_r} & 0\\ 0 & K_{b_r}\end{bmatrix} \\ - \hat{\imath}\Omega\begin{bmatrix}C_{b_r} & 0\\ 0 & C_{b_r}\end{bmatrix} - \hat{\imath}\Omega\eta_r\left(\begin{bmatrix}\alpha K & 0\\ 0 & \beta K\end{bmatrix}\right. \\ \left.\left. + \begin{bmatrix}\alpha K_{b_r} & 0\\ 0 & \beta K_{b_r}\end{bmatrix}\right)\right)\begin{Bmatrix}q_1\\ \bar{q}_2\end{Bmatrix} \\ = \begin{Bmatrix}f_x + \hat{\imath}f_y\\ 0\end{Bmatrix}(\Omega^2 - \hat{\imath}\dot{\Omega})e^{\hat{\imath}\Omega t}\end{aligned} \tag{19}$$

Here α and β are scalar values defined by

$$\alpha = \frac{1}{|\omega-\Omega|}, \qquad \beta = \frac{1}{|-\omega-\Omega|} \tag{20}$$

In Equation (19), overbar represents the complex conjugate terms. The obtained equation provides a mathematical

explanation for some of the key features of rotating systems, with the help of complex coordinates approach and is represented for the first time in this study. The total vibratory response of the system now forms an ellipse. The upper half of the matrices represent forward whirl and lower half represent backward whirl. Note that although only forward modes are excited in the upper half of the system matrices, there will be a response in the lower half of the system due to couplings. This explains the excitation of the backward modes under forward rotating unbalance loads when asymmetric supports are used. Moreover, rotor matrices, including rotating bearing stiffness and damping, do not have mean and deviatoric terms since rotor itself is isotropic. In the second row of the equation, the complex conjugate of mean and deviatoric matrices is included to account for backward rotating terms. Different sign notations based on absolute value function are used in both rows to calculate relative frequency of the structural damping, since each row represents opposite whirl directions. These absolute value functions associated with the structural damping terms introduce kinematic nonlinearity to the system, which is not suitable for eigenvalue calculation. Therefore, the homogeneous equation is repeatedly solved for all possible sign configurations to overcome this situation, which causes a significant increase in computational time when structural damping is employed. Furthermore, despite the publication of some results with structural damping and anisotropic supports [20], the equation of the motion is not clearly explained in the literature until now. Equation (19) provides a framework allowing the incorporation of structural damping, anisotropic supports, bearings with cross-coupling stiffness, and rotor-rotor bearings into a unified model which contributes to a more comprehensive understanding of the dynamic behavior of the system.

4. The Case Study

The stability of the rotor shown in Figure 2 is studied for various configurations with different support and internal damping characteristics. The rotor system consists of a 3 m hollow shaft mounted on two ends. There are five disks connected to the shaft with interference fit. The rotor operates up to 6000 RPM, and material properties of the disks and shaft are provided in Table 1.

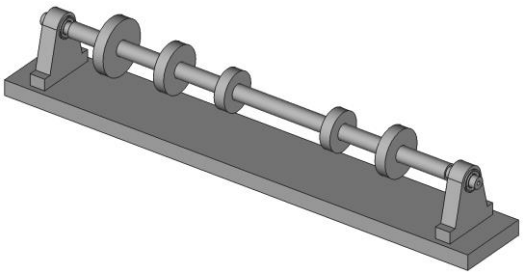

Figure 2. The schematic of rotor with five disks and two bearings.

Table 1. Material properties of the rotor.

Modulus of Elasticity, (MPa)	211000
Shear Modulus, (MPa)	81200
Density, (kg/m^3)	7810
Structural Damping Coefficient	0.001

The considered rotor is modelled with 30 shaft elements in the developed model. The schematic of the model used to study the stability of the system is shown in Figure 3. The corresponding geometric properties of the shaft elements are also provided in Table 2.

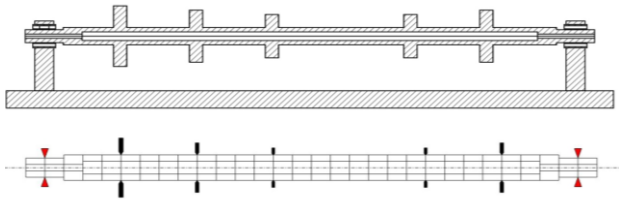

Figure 3. Schematic of the finite element model of the rotor with five disks and a bearing at each end.

Table 2. Geometric properties of shaft elements.

Element #	Length, m	Outer Diameter, m	Inner Diameter, m
1 and 2	0.1	0.075	0.025
3	0.1	0.1	0.025
4 to 27	0.1	0.1	0.05
28	0.1	0.1	0.025
29 and 30	0.1	0.075	0.025

Moreover, disks on the rotor are considered as rigid concentrated masses in the developed model with geometric properties provided in Table 3.

Table 3. Geometric properties of disk elements.

Disk #	Axial Positions, m	Inner Diameter, m	Outer Diameter, m	Thickness, m
1	0.5	0.1	0.35	0.07
2	0.9	0.1	0.3	0.07
3	1.3	0.1	0.25	0.07
4	2.1	0.1	0.25	0.07
5	2.5	0.1	0.3	0.07

The analysis will be repeated for different cases of support bearing stiffness, type of disk connection, and structural damping. Accordingly, four different configurations with corresponding details are provided in Table 4. Analysis will show the effect of support stiffness, internal damping due to interference fits and structural damping, on both computational time and vibrational stability.

Table 4. Mount and Internal Damping Characteristics.

Case #	Mount Stiffness	Mount Damping	Disk Connection	Structural Damping
1	Isotropic k = 5e6 N/m	5 N-s/m	Rigid	0
2	Anisotropic k_x = 4e6 N/m, k_y= 5e6 N/m	5 N-s/m	Rigid	0
3	Anisotropic k_x = 4e6 N/m, k_y = 5e6 N/m	5 N-s/m	k = 1e8 N/m, k_r =6e5 N-m/rad c_r = 200 N-m-s/rad	0
4	Anisotropic k_x = 4e6 N/m, k_y = 5e6 N/m	5 N-s/m	k = 1e8 N/m, k_r =6e5 N-m/rad c_r = 200 N-m-s/rad	0.001

Furthermore, the same model is also created in commercial finite element software, Ansys 2024R1, as shown in Figure 4. General axisymmetric Solid272 elements with four nodal planes are used to model the rotor parts, as shown in Figure 5. This element type supports both gyroscopic and circulatory matrices and provides accuracy similar to 3D solid elements with less computation time. There are 573 elements and 2904 nodes in the model. Combi250 bushing elements are used to define the stiffness and damping characteristics of the mounts. MPC184 general joint elements are used to define the flexible connection between the disks to the shafts. Rotating viscous damping representing the interference fit is defined with a Beta Damping Coefficient, which will result in the same viscous damping provided in Table 4. Full Damped solver is used for modal solution. The Coriolis effect is activated to include gyroscopic effects and rotating damping matrix is activated to include circulatory effects.

Figure 4. 3D finite element model of the rotor with five disks in Ansys.

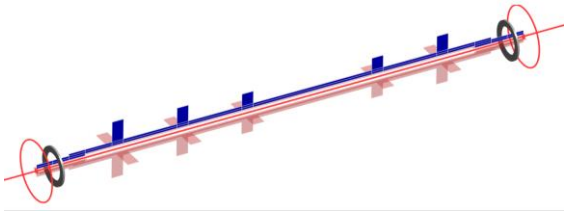

Figure 5. Nodal planes of solid272 elements used in ANSYS model.

5. Results and Dicussion

At the first step, to verify the model, obtained natural frequencies based on the developed models are compared to those of the ANSYS model. The results of the first six modes are reported in Table 5 for different values of rotor speed and case studies. It can be seen that there is acceptable agreement between the results. The maximum relative differences between the results for cases #1 to #4 are respectively, 3.95%, 3.64%, 2.52%, and 2.51%. The average relative differences between the results for cases #1 to #4 are also 2.60%, 2.52%, 1.41%, and 1.42%, respectively.

Table 5. Comparison of the first six natural frequencies of the rotor to the ANSYS results for different rotor speeds and case studies.

Rotor speed (RPM)	Case study #	Models	Natural Frequencies (Hz) for mode #					
			1	2	3	4	5	6
1000	1	Present	16.679	16.779	42.326	42.431	78.758	79.648
		ANSYS	17.321	17.403	43.176	43.274	80.539	81.425
	2	Present	16.123	16.733	39.116	42.380	74.320	79.255
		ANSYS	16.685	17.364	39.762	43.226	76.094	81.024
	3	Present	16.108	16.720	38.867	42.061	72.974	77.638
		ANSYS	16.247	16.871	39.241	42.543	74.567	79.506
	4	Present	16.108	16.716	38.867	42.061	72.974	77.637
		ANSYS	16.247	16.871	39.241	42.543	74.567	79.506
3000	1	Present	16.579	16.878	42.218	42.539	77.721	80.697
		ANSYS	17.239	17.484	43.077	43.371	79.660	82.319
	2	Present	16.096	16.758	39.108	42.389	73.950	79.652
		ANSYS	16.669	17.379	39.755	43.231	75.793	81.340
	3	Present	16.078	16.738	38.851	42.061	72.244	77.969
		ANSYS	16.224	16.887	39.229	42.543	73.933	79.798
	4	Present	16.077	16.738	38.851	42.061	72.244	77.968
		ANSYS	16.224	16.887	39.229	42.543	73.933	79.798
5000	1	Present	16.478	16.975	42.109	42.645	76.758	81.704
		ANSYS	17.156	17.564	42.978	43.469	78.789	83.219
	2	Present	16.047	16.805	39.092	42.400	73.335	80.302
		ANSYS	16.637	17.408	39.743	43.241	75.278	81.886
	3	Present	16.019	16.777	38.821	42.063	71.023	78.458
		ANSYS	16.181	16.916	39.204	42.545	72.855	80.251
	4	Present	16.020	16.776	38.821	42.063	71.024	78.457
		ANSYS	16.181	16.916	39.204	42.545	72.855	80.251

After verifying the model, the detailed modal results are provided for the rotor of case #1. This configuration has isotropic mounts and there is no internal instability source defined. Accordingly, Campbell diagram and decay rates for this rotor are shown in Figure 6. In Figure 6a, the forward whirls are shown by red solid lines, backward whirls are depicted by blue dash-dotted lines, and the 1X is shown by purple dashed line. It can be seen that the first backward and forward critical speeds of the rotor are predicted to be around 1001 and 1007 RPM, respectively, and decay rates predict stable operation up to 6000 RPM. However, decay rate values imply that the system is lightly damped and may experience high vibrations during operation.

Moreover, the first three mode shape couples of case #1 based on the current method and Ansys are provided in Figure 7 and Figure 8, respectively, to show that each method predicts similar vibration patterns. The number of nodal points in each results set are the same for corresponding mode shapes. Deflection of rotor axis in these deformed shapes is the main reason for emergence of gyroscopic moments in lateral vibrational mode shapes. These mode shapes are observed in backward and forward couples due to the presence of gyroscopic moments. Accurate prediction of mode shapes and nodal points are critical in the selection of excitation locations. It can be also seen that mode shapes are circular since case #1 has mount stiffness in both lateral planes. Whirl orbits will become elliptical when mount stiffness becomes asymmetric.

Case #2 introduces support anisotropy to the system. Similarly, modal results based on Campbell diagram and stability map are provided in Figure 9. Natural frequencies of the system are not paired in pure forward and backward mode couples anymore. In Figure 9a, the forward whirls are shown by red solid lines, backward whirls are depicted by blue dash-dotted lines, mixed whirls are shown by black dotted lines, and the 1X is shown by purple dashed line. Comparison of the decay rate plots shown in Figures 6 and 9 shows the improvement in the stability of the system due to the support anisotropy. The first backward and

forward critical speed of the system are predicted as 967, and 1004 RPM, respectively, which is slightly below case #1 due to the reduction in the support stiffness in one of the lateral directions.

In cases #1 and #2, disks are assumed to be connected rigidly to the shaft. Since there is no relative motion in mating surfaces, no internal damping is produced. Case #3 however, introduces internal damping due to interference fit joints. Campbell diagram and stability map of this configuration are provided in Figures 10a and 10b, respectively. Note that there is negligible change in the Campbell diagram of the system when compared to Case #2 and the critical speed is again around 966 and 1003 RPM. On the other hand, there is a significant difference in the stability characteristics of the system. When internal damping terms are introduced to the system as viscous rotational damping of rotating bearings between disks and shaft, system becomes unstable after 5280 RPM. This is the stability threshold of the system. Any initial vibrations beyond this speed will be amplified and will result in catastrophic failure in the rotor.

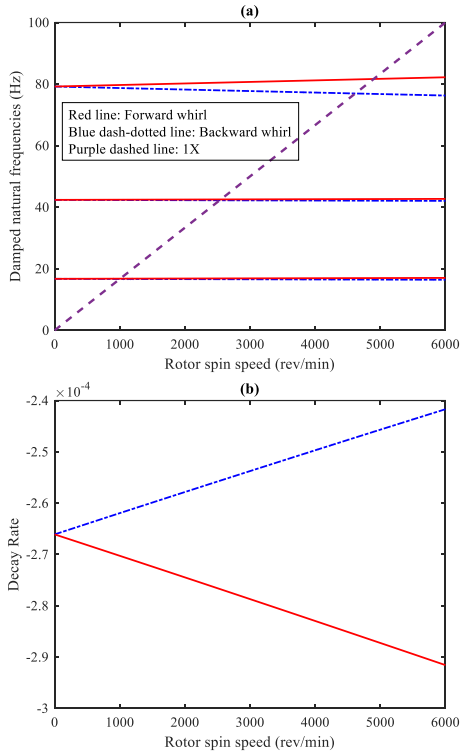

Figure 6. (a) Campbell diagram, and **(b)** decay rates of the first forward and backward whirls (stability map) for the rotor of case #1.

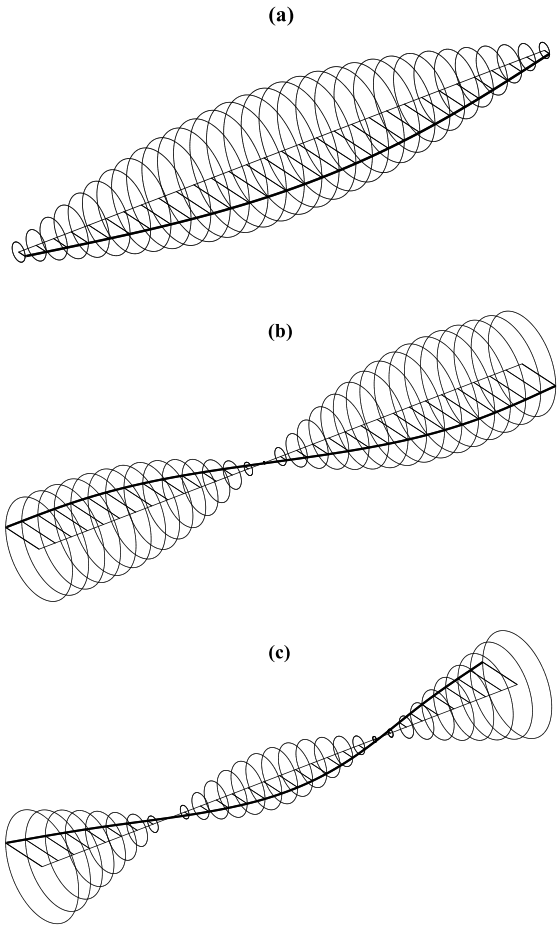

Figure 7. (a) First, **(b)** Second, and **(c)** Third mode shape couples for the rotor of case #1 based on the present method.

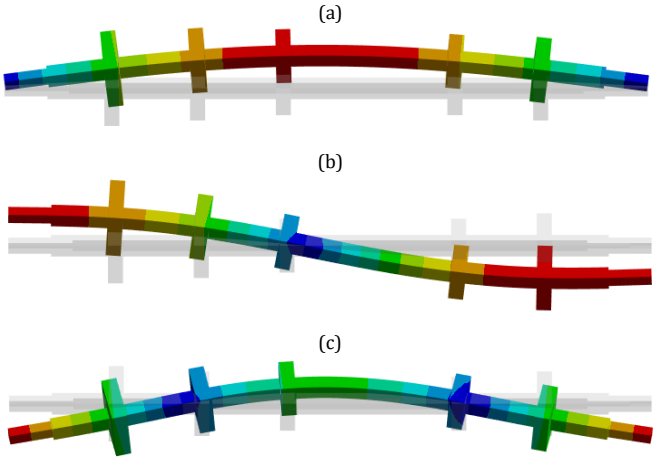

Figure 8. (a) First, **(b)** Second, and **(c)** Third mode shape couples of the rotor of case #1 based on model in Ansys.

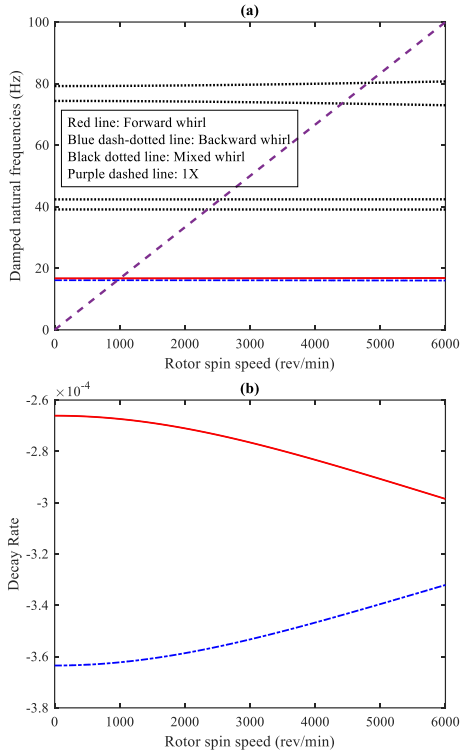

Figure 9. (a) Campbell diagram, and **(b)** decay rates of the first forward and backward whirls (stability map) for the rotor of case #2.

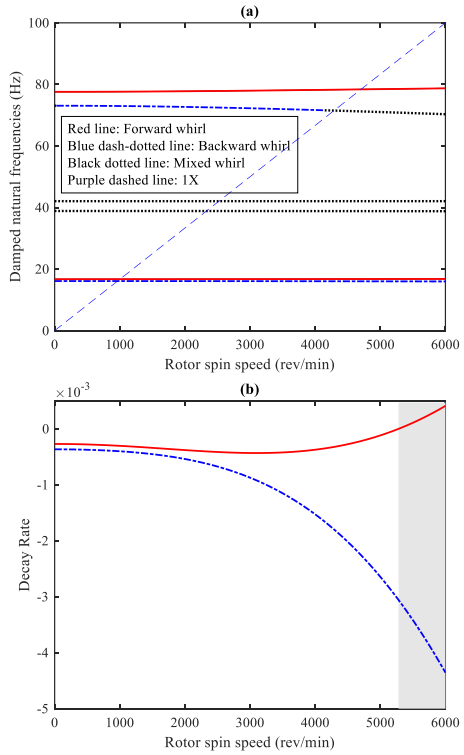

Figure 10. (a) Campbell diagram, and **(b)** decay rates of the first forward and backward whirls (stability map) for the rotor of case #3, (Gray area: unstable region).

Finally, structural damping is introduced to the system in case #4. The structural damping coefficient of both rotor and stator is assumed as 0.001. Again, no difference is observed in the Campbell diagram of the system, as shown in Figure 11a. The first critical speeds of case #4 are also 966 and 1003 RPM, for first backward and forward modes, respectively. However, there are sudden changes in the stability of the system when critical speeds are exceeded, which is expected for rotors with internal structural damping [19]. It is important to note that in Figure 11b, the stability threshold of the system decreases to 4370 RPM when internal structural damping is introduced in addition to the internal damping of interference fit regions.

In order to analyze the efficiency of the developed model, computational times for all four cases based on the current model are provided in Table 6 and compared to those of the classical finite element model developed by Friswell [26]. According to this table, isotropic systems yield the quickest solutions as matrix sizes are halved using the complex coordinates approach. However, this advantage is lost in case #2 when anisotropic supports are introduced to the system. In case #3, the addition of rotating bearing elements between disks and shafts causes a further slight increase in computational time. Case #4 requires the longest computational time since eigenvalue calculation is repeated for different sign configurations because of nonlinearity induced by structural damping.

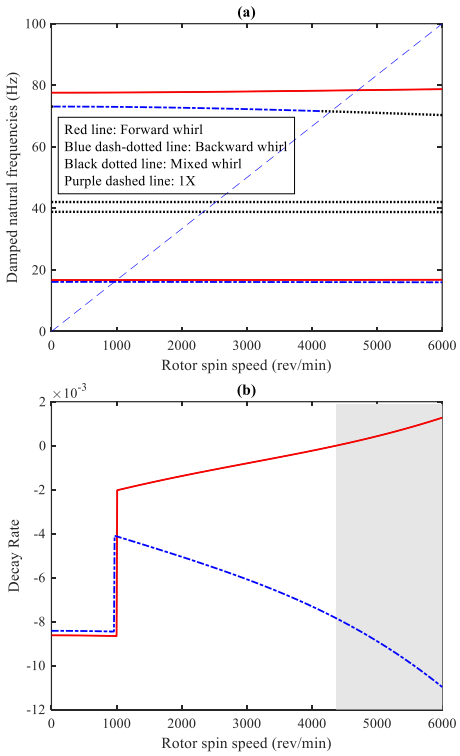

Figure 11. (a) Campbell diagram, and **(b)** decay rates of the first forward and backward whirls (stability map) for the rotor of case #4 (Gray area: unstable region).

Table 6. Computational Times.

Case #	Complex coordinates formulation	Real coordinates formulation [26]
1	5.6 sec	25.8 sec
2	24.9 sec	25.5 sec
3	36.3 sec	-
4	146.7 sec	-

6. Conclusions

A finite element model based on Timoshenko shaft elements with complex coordinates formulation was developed to accurately predict the internal stability of rotordynamic systems. The equations of motion for rotors on isotropic and anisotropic

supports are provided, with a focus on the complexities introduced by circulatory terms induced by internal damping. Internal damping does not always have a stabilizing impact on vibrations like external damping, since the two experience different vibration frequencies with respect to stationary reference frame. The study considered two primary sources of internal instability. The first involves frictional joints between rotor parts, such as axial splines, interference fits, and curvic couplings. The second major source is hysteresis damping of the rotor material. The former is defined by rotating viscous damping, while the latter is characterized by a structural damping coefficient. The paper discussed the challenges and controversies surrounding the normalization of structural damping in rotordynamic literature and emphasizes the need for accurate modeling to achieve a unified approach in studying internal rotordynamic stability. A case study to demonstrate the application of the developed method is presented. Four different configurations were analyzed, considering isotropic and anisotropic supports, internal damping due to interference fits, and structural damping. Natural frequencies, critical speeds and decay rates are obtained by solving the developed model. The results showed varying stability thresholds and computational times for each configuration. In summary, this study contributes to the understanding of internal rotordynamic stability, providing a robust methodology for accurate modeling and analysis.

Nomenclature

s	Stationary (Subscript)
r	Rotating (Subscript)
b	Bearing (Subscript)
η	Loss Factor
c_{eq}	Equivalent Damping Ratio
ω	Vibration Frequency
Ω	Rotor Speed
u, v	Translational Deformations
ψ, θ	Angular Deformations
U	Potential Energy
T	Kinetic Energy
E	Modulus of Elasticity
ρ	Density
ν	Poisson Coefficient
A	Area of Shaft Cross Section
I	Second Moment of Shaft Cross Section
l	Shaft Element Length
r_i	Shaft Inner Radius
r_o	Shaft Outer Radius
χ	Shear Factor
Φ	Slenderness Ratio
J	Mass Moment of Inertia
q	Deformation Vector
f	Force Vector
M	Mass Matrix
C	Damping Matrix
G	Gyroscopic Matrix
K	Stiffness Matrix
N	Shape Function Matrix

Ethics committee approval and conflict of interest statement

This article does not require ethics committee approval. This article has no conflicts of interest with any individual or institution.

Author Contribution Statement

Author1: Conceptualization, Methodology, Software, Validation, Visualization, Writing – original draft.

Ahuthor 2: Conceptualization, Validation, Supervision, Writing – review & editing.

References

[1] Wu, J., Rezgui, D., Titurus, B. 2023. Model and experimental analysis of a rotor rig dynamics with time-varying characteristics, Journal of Sound and Vibration, Vol. 557, pp. 117683.

[2] Lotfan, S., Salehpour, N., Adiban, H., Mashroutechi, A., 2015. Bearing fault detection using fuzzy C-means and hybrid C-means-subtractive algorithms. IEEE International Conference on Fuzzy Systems (FUZZ-IEEE), August, Istanbul, pp.1–7.

[3] Pattnayak, M., Dutt, J., Pandey, R., 2022. Rotordynamics of an accelerating rotor supported on aerodynamic journal bearings. Tribology International, Vol.176, pp.107883.

[4] Lotfan, S., Bediz, B., 2022. Free vibrations of rotating pre-twisted blades including geometrically nonlinear pre-stressed analysis. Journal of Sound and Vibration, Vol.535, pp.117109.

[5] Chipato, E.T., Shaw, A.D., Friswell, M.I., 2021. Nonlinear rotordynamics of a MDOF rotor–stator contact system subjected to frictional and gravitational effects. Mechanical Systems and Signal Processing, Vol.159, pp.107776.

[6] De Felice, A., Sorrentino, S., 2021. Damping and gyroscopic effects on the stability of parametrically excited continuous rotor systems. Nonlinear Dynamics, Vol.103, pp.3529–3555.

[7] Lotfan, S., Anamagh, M.R., Bediz, B., Cigeroglu, E., 2022. Nonlinear resonances of axially functionally graded beams rotating with varying speed including Coriolis effects. Nonlinear Dynamics, Vol.107, pp.533–558.

[8] Krack, M., Salles, L., Thouverez, F., 2017. Vibration prediction of bladed disks coupled by friction joints. Archives of Computational Methods in Engineering, Vol.24, pp.589–636.

[9] Lund, J.W., 1967. Destabilisation of rotors from friction in internal joints. In: Vibration and Wear in High Speed Rotating Machinery, pp.617–629.

[10] Walton, J., Artiles, A., Lund, J., Dill, J., Zorzi, E., 1990. Internal rotor friction instability. NASA Report, Vol. NAS 1.26: 183942.

[11] Wang, L., Wang, A., Jin, M., Yin, Y., Heng, X., Ma, P., 2021. Nonlinear dynamic response and stability of a rod fastening rotor with internal damping effect. Archive of Applied Mechanics, Vol.91, pp.3851–3867.

[12] Dai, Z., Jing, J., Chen, C., Cong, J., 2018. Extensive experimental study on the stability of rotor system with spline coupling. In: Turbo Expo: Power for Land, Sea, and Air, Vol.51135, pp.V07AT33A021.

[13] Melanson, J., Zu, J., 1998. Free vibration and stability analysis of internally damped rotating shafts with general boundary conditions. ASME Journal of Vibration and Acoustics, Vol.120, pp.776–783.

[14] Genta, G., Brusa, E., 2000. On the role of nonsynchronous rotating damping in rotordynamics. International Journal of Rotating Machinery, Vol.6, pp.467–475.

[15] Forrai, L., 2000. A finite element model for stability analysis of symmetrical rotor systems with internal damping. Journal of Computational and Applied Mechanics, Vol.1, pp.37–47.

[16] Cerminaro, A.M., Nelson, F.C., 2000. The effect of viscous and hysteretic damping on rotor stability. In: Turbo Expo: Power for Land, Sea, and Air, Vol.78576, pp.V004T03A043.

[17] Ku, D.-M., 1998. Finite element analysis of whirl speeds for rotor-bearing systems with internal damping. Mechanical Systems and Signal Processing, Vol.12, pp.599–610.

[18] Genta, G., 2004. On a persistent misunderstanding of the role of hysteretic damping in rotordynamics. ASME Journal of Vibration and Acoustics, Vol.126, pp.459–461.

[19] Genta, G., Amati, N., 2010. Hysteretic damping in rotordynamics: An equivalent formulation. Journal of Sound and Vibration, Vol.329, pp.4772–4784.

[20] Genta, G., 2015. On the stabilizing effect of support asymmetry in rotordynamics. In: Proceedings of the 9th IFToMM International Conference on Rotor Dynamics, Springer, pp.2045–2057.

[21] d'Alessandro, F., Festjens, H., Chevallier, G., Cogan, S., 2021. Hysteretic damping in rotordynamics: A focus on damping induced instability. IMAC XL, SEM, February, Orlando, FL, USA.

[22] Chandra, N.H., Sekhar, A., 2016. Nonlinear damping identification in rotors using wavelet transform. Mechanism and Machine Theory, Vol.100, pp.170–183.

[23] Kozioł, M., Cupiał, P., 2022. The influence of the active control of internal damping on the stability of a cantilever rotor with a disc. Mechanics Based Design of Structures and Machines, Vol.50, pp.288–301.

[24] Mori, H., Sueda, M., Shiroshita, K., Kondou, T., 2024. Effect of damping and rotor moment of inertia on stability of self-synchronization for two unbalanced rotors. Journal of Sound and Vibration, Vol.570, pp.118103.

[25] Arab, S.B., Rodrigues, J.D., Bouaziz, S., Haddar, M., 2018. Stability analysis of internally damped rotating composite shafts using a finite element formulation. Comptes Rendus Mécanique, Vol.346, pp.291–307.
[26] Friswell, M.I., 2010. Dynamics of Rotating Machines. Cambridge University Press.
[27] Roy, D.K., Tiwari, R., 2019. Development of identification procedure for the internal and external damping in a cracked rotor system undergoing forward and backward whirls. Archive of Mechanical Engineering, Vol.66, pp.229–255.
[28] Mendonça, W.R.D.P., De Medeiros, E.C., Pereira, A.L.R., Mathias, M.H., 2017. The dynamic analysis of rotors mounted on composite shafts with internal damping. Composite Structures, Vol.167, pp.50–62.
[29] Zorzi, E., Nelson, H., 1977. Finite element simulation of rotor-bearing systems with internal damping. ASME Journal of Engineering for Power, Vol.99, pp.71–76.
[30] Nelson, H., 1980. A finite rotating shaft element using Timoshenko beam theory. ASME Journal of Mechanical Design, Vol.102(4), pp.793–803.
[31] Genta, G., 2005. Dynamics of Rotating Systems. Springer Science & Business Media.
[32] Rezaee, M., Lotfan, S., 2015. Non-linear nonlocal vibration and stability analysis of axially moving nanoscale beams with time-dependent velocity. International Journal of Mechanical Sciences, Vol.96, pp.36–46.
[33] Farshbaf Zinati, R., Rezaee, M., Lotfan, S., 2020. Nonlinear vibration and stability analysis of viscoelastic Rayleigh beams axially moving on a flexible intermediate support. Iranian Journal of Science and Technology, Transactions of Mechanical Engineering, Vol.44, pp.865–879.
[34] Lotfan, S., Sadeghi, M.H., 2017. Large amplitude free vibration of a viscoelastic beam carrying a lumped mass–spring–damper. Nonlinear Dynamics, Vol.90, pp.1053–1075.